heritage

MDPI

Article

Multianalytical Study of a Painting on Copper

Roberta Iannaccone [1,*], Alessandro Ponzeletti [2], Giovanni Bartolozzi [3], Luca Malfatti [4] and Antonio Brunetti [4,*]

[1] Dipartimento di Scienze Chimiche, Fisiche, Matematiche e Naturali, Università degli Studi di Sassari, Via Vienna 2, 07100 Sassari, Italy
[2] Dipartimento Arti Visive, Accademia delle Belle Arti di Sassari, Via Duca degli Abruzzi 4, 07100 Sassari, Italy; alessandroponzeletti@accademiasironi.it
[3] Istituto di Fisica Applicata Nello Carrara, Via Madonna del Piano 10, 50019 Sesto Fiorentino, Italy; g.bartolozzi@ifac.cnr.it
[4] Dipartimento di Scienze Biomediche, Università degli Studi di Sassari, Viale San Pietro, 07100 Sassari, Italy; luca.malfatti@uniss.it
* Correspondence: riannaccone@uniss.it (R.I.); brunetti@uniss.it (A.B.)

Abstract: The painting studied, featuring the Virgin contemplating the sleeping Child, is a well-known composition in the religious context, especially popular since the 16th century. The technique, oil on copper plate, and materials were examined applying a multimethodological non-invasive approach. The main goal was to quantitatively characterize the layer composition and thickness. To obtain them, X-ray fluorescence spectroscopy coupled with Monte Carlo simulation was used for the first time, to the best of our knowledge, for this kind of object. This technique was also integrated with more conventional photographic and spectroscopic techniques such as multiband imaging (MBI), Raman spectroscopy, external reflection Fourier transform infrared spectroscopy (ER FT-IR), and optical microscopy. The obtained data showed the use of a background based on lead white, a wide palette, which includes azurite, vermilion, lead white, and some ochers, and documented the conservation status. Although the investigations contended with the object's complexity, the results demonstrate the efficacy of the XRF–Monte Carlo simulation approach in characterizing the materials constituting the artwork in a totally non-invasive way.

Keywords: painting on copper; XRF; Monte Carlo simulation; multiband imaging; ER FT-IR; Raman

Citation: Iannaccone, R.; Ponzeletti, A.; Bartolozzi, G.; Malfatti, L.; Brunetti, A. Multianalytical Study of a Painting on Copper. *Heritage* **2024**, *7*, 301–323. https://doi.org/10.3390/heritage7010015

Academic Editor: Kerstin Elert

Received: 2 December 2023
Revised: 31 December 2023
Accepted: 5 January 2024
Published: 9 January 2024

1. Introduction

The artwork analyzed belongs to the class of peculiar paintings on a copper plate. The distinctive features of these oil paintings, which became popular in the 16th century in Italy and then were largely adopted by northern European artists, lie in the metal support, a slab of almost pure copper [1].

The painters believed that the copper substrate was less susceptible to expansions and structural movements compared to canvas and wood panels and therefore less inclined to create the fine pattern of cracking on the surface, called craquelure [2]. This technique, apart from a few famous artists such as Bronzino, Carracci, and Reni, was used for medium–small formats, targeted for private devotional use, and is still used for small artisanal workmanship.

The painting, by an anonymous artist probably from the north of Italy, is dated back to the first quarter of the 17th century and belongs to a private collection (Figure 1). The small dimensions of the painting (16.5 × 12.0 cm) suggest a personal purpose as a devotional object.

The composition shows an intimate scene with the Virgin contemplating the Child while sleeping in a bed on a uniform background.

Figure 1. The Virgin and the sleeping Child.

The iconography recalls a well-known representation which finds, among its first famous example, the Virgin and the sleeping Child in the *Pala Montefeltro*, also called *Pala di Brera*, by Piero della Francesca [3] painted between 1472 and 1474 [4].

Before the famous *Pala Montefeltro*, the presence of the same iconography in other paintings by less famous artists cannot be excluded. However, due to the fame of Piero della Francesca, the composition became very popular and found different elaborations among later painters and was used both in paintings and graphics. The sleeping Child is related to the symbolic value of Christ's fate. In this context, sleep is related to death but also the reawakening and Christ's resurrection after death. This symbolic connection with Christ's fate is once more emphasized in Piero della Francesca's painting, by the red coral on the child's neck symbolizing the red blood of crucifixion.

The subject was then elaborated, in the 16th century, giving it a more intimate connotation: the Child sleeping on a bed or crib, with the head oriented to the left or right side and covered with a blanket or a bedsheet, with a decoration that can vary from simple up to a golden one. The Virgin usually has a central role in the composition, but she is placed in the background while contemplating the Child with hands joined in prayer.

Multiple versions exist, showing the sleeping Christ Child, and the subject was widely spread by Ordine dei Gesuiti in the New World, especially in South America where these kinds of representation still take hold in the traditional painter school of Cuzco (Peru) [5].

From the point of view of the composition, the painting analyzed recalls the works of the Flemish engraver Hieronymus Wierix [6–8] made before 1619 and stored at the British Museum of London [9]. The Wierix work, which revisited the iconography of the Virgin Mary contemplating her son repeatedly, was probably the inspiration for the anonymous painter.

A first examination with raking light showed the presence of an irregular surface due to the thin copper plate and the presence of mechanical damages probably due to an impact, especially noticeable at the corners, where the loss of pigment was easily detectable [10] (Figure 2). However, excluding the edges, the surface showed only small gaps and scratches, while diffuse corrosion brown spots were visible in the lighter areas highlighted by the observation of the NIR image (Figure 2).

(**a**) (**b**)

Figure 2. The presence of an irregular surface is highlighted by (**a**) raking light image, while retouches are visible in (**b**) the NIR 1 image of the painting.

A few small retouches were visible when observing the surface with the portable optical microscope, excluding the edges where extended retouches were evident to the naked eye and mapped with the NIR images.

2. Materials and Methods

2.1. X-ray Fluorescence with Monte Carlo Simulation

Our study is based on a novel approach for this type of painting, utilizing X-ray fluorescence measurements (referred to hereafter as XRF) integrated with a Monte Carlo simulation of the same experiment. This technique enabled us to characterize the painting's structure (support, preparatory layer, and painting) in terms of both elemental composition and layers thickness. Furthermore, to characterize the spatial distribution and composition of the compounds and degradation products, this technique was integrated with other non-invasive techniques: MSI, ER FT-IR, and Raman spectroscopy.

The peculiarity of the support, with its completely different hardness compared with the painting layer, and the thickness of the painting layer itself, discouraged the use of invasive techniques involving sampling. Additionally, employing a multimethodological protocol allowed us to address the potential limitations of each technique by correlating different data and leveraging their complementarity, namely XRF, Monte Carlo simulation, and micro XRF.

To quantify the composition of the sample, several analytical approaches have been developed, where the fundamental parameters method [11–14], is the most used. In the case of the metallic multilayered approach, an alternative method has been proposed based on the relative changes in the attenuation of some specific elements [15–17]. This approach is easy and fast to use but it is strongly dependent on the sample. However, in the case

of complex samples with multilayered structures and/or irregular surfaces, an analytical approach is not always the best solution for the quantification of their chemical content.

In the last decades, alternative approaches have been proposed, mainly based on the use of a Monte Carlo simulation of the real experiment [18–23]. A Monte Carlo simulation is based on a probabilistic approach to the phenomenon to be reproduced. It is used when a problem has a high number of variables, and the analytical approach is computationally too intensive or impractical to implement. As a result of this simulation, an X-ray spectrum is produced. The real and the simulated spectra are compared. The simulation protocol can be divided into two parts: the first part (verconcerns the modeling of the experimental setup and is carried out once, while the second part involves the quantification procedure itself. The setup characterization includes:

- Determining the real X-ray emission, which is arguably the most important step due to its influence on the performance of the simulation.
- Describing the measurement geometry.
- Determining the X-ray detector response in terms of both energy efficiency and energy resolution, with the latter including the shape of the peak.

The quantification protocol consists of the following steps:

1. Creating a preliminary model of the sample, considering both its layer structure and composition. This step is primarily based on the peaks observed in the XRF spectrum and a visual inspection of the sample, including its colors in the picture or the results of multiband photographic analysis.
2. Performing a simulation of the measurement.
3. Comparing the experimental and simulated spectra.
4. If any discrepancies are observed, adjusting the sample's structure or composition and repeating steps b and c. The estimation of the "discrepancy" is initially based on visual inspection and is then refined using a chi-squared test.

The Monte Carlo code used here is a fast one named XRMC [20,21], based on the Xraylib atomic database [22,23]. It can produce a spectrum with quality comparable to that measured in less than 20 s when running on a standard laptop. A more complete description of the Monte Carlo technique applied to cultural heritage can be found in [24]. The main advantage of using a Monte Carlo simulation, besides the possibility of simulating complex structures, lies in the absence of the need to remove the background from the X-ray spectrum in order to estimate the areas of the peaks, as required by standard quantitative techniques such as the aforementioned fundamental parameter method. Background removal implies the use of analytical methods, such as fitting functions or other mathematical operators [25–27]. As a result of the removal process, the peak areas superimposed on the background can be altered, potentially leading to incorrect, either overestimated or underestimated, values for the corresponding chemical element. The error in estimating the background beneath the peak affects smaller area peaks, which correspond to chemical elements with lower concentrations, reducing the minimum detectable concentration. For this reason, even with portable XRF instruments, the use of a Monte Carlo simulation with XRF measurements allows for an improvement in the detection limit, from about 100–200 ppm down to about 20 ppm depending on the chemical element considered. Regarding the error in the estimation of the chemical contents, it depends not only on the error in fitting the X-ray spectrum, but also on the error in the values of the atomic parameters used for quantification. As a rule of thumb, it ranges from 2% to 10%, where the worst values are for the low concentration elements and/or for the external fluorescence line, i.e., from M-lines onwards. To validate the performance of the Monte Carlo software (ver. 6.4.1), we evaluated it by comparing it with another Monte Carlo code that has been tested in simulating experimental measurements of certified samples [24].

The experimental apparatus was composed of an SDD detector (1-2-3 SDD by Amptek, Bedford, MA, USA) and a rhodium anode X-ray tube working at 40 kV 5–15 μA (Amptek, USA). The X-ray tube output was collimated by a 1 mm wide cylindrical collimator while

the detector was used without any collimation/filter. The detector was placed vertically on the surface and the X-ray tube formed a 30° angle with respect to the detector, both positioned 2–3 cm away from the surface. This arrangement allowed to minimize the effects on the measured spectrum due to the roughness of the painted surface. The spot size was about 2 mm^2 in diameter. All the measurements were performed in the air. The choice of the working voltage depended on two constraints: the power of the X-ray tube and the availability of a model of the X-ray spectrum emitted by the X-ray tube and used in the simulations. The X-ray spectrum was not filtered in order to use the information contained in the background that was mainly connected to the sample's composition part without any detectable fluorescence signal, such as the elements with low atomic numbers. Each spectrum was acquired for about 4–6 minutes or until a good statistic spectrum was obtained. Both the acquisition/control and the Monte Carlo software (XRMC ver 6.7.0) ran on an Intel I7-based laptop, thus making the instrumentation completely portable.

For the type of object examined in this paper, a multilayered model was chosen and several combinations tested. However, the best results were obtained with a three-layer model: a painting layer, a preparatory layer, and a copper support.

It is important to emphasize the influence of voids (pores) caused, for example, by corrosion phenomena, on the determination of thickness. In fact, the attenuation of X-rays traveling through a medium follows the Lambert–Beer law:

$$I(E) = I_0 \, e^{-\mu(E,Z)x}$$

where:

E is the photon energy and Z the atomic number;
I is the number of photons detected;
I_0 is the number of photons emitted by the X-ray source;
$\mu(E,Z)$ is the so-called linear absorption coefficient;
x is the path traveled inside the sample.

The presence of pores inside a material virtually changes the value of the linear absorption coefficient μ, because part of the material is replaced by air that has a lower μ value. If the Monte Carlo model of the sample considers a uniformly filled layer instead of a real porous layer, this will produce a thicker estimation of the model (a longer path); thus, when the model is created, this aspect must be considered.

To obtain information on the distribution of elements in the tiny decorative areas, μ-XRF with M4 Tornado (Bruker, Ettlingen, Germany) was used. The X-ray Rh tube can operate between 10 and 50 kV and 100–600 μA, with the option to also choose a polycapillary lens to obtain a spot size down to 25 μm. Detection of fluorescence radiation was performed by an energy-dispersive SDD with a sensitive area of 30 mm^2 and an energy resolution of 142 eV for Mn Kα. The analysis was conducted under vacuum conditions (20 mbar) to collect X-ray fluorescence from elements with low atomic numbers, at 50 kV and 30 μA. The instrument also allows for the acquisition of maps of selected areas. The maps were acquired with a scan resolution of 600 × 600 pixels. No primary filter was used, and acquisitions were set to 300 s. In this case, Monte Carlo simulations were not applied due to the absence of a model for the polycapillary lens and, more importantly, because the error in the focusing distances of the instruments was of the same order of magnitude as the maximum distance of origin of fluorescence photons. Thus, a multilayer structure would have been unhelpful.

2.2. Multiband Imaging

The techniques used included ultraviolet reflected (UVR), ultraviolet false color (UVFC), ultraviolet-induced visible luminescence (UVL), visible (VIS), visible-induced luminescence (VIL), reflected near-infrared (NIR), and infrared reflected false color (IRRFC) photography [28–31].

In addition, for the investigation of the surface of the painting, acquisitions with raking light at different angles were conducted.

For the analyses, a digital camera D850 (Nikon, Tokyo, Japan), featuring a CMOS sensor 35.9 × 23.9 mm, with the removal of the inner ICF/AA filter [32] and 45.7 Mpixel, equipped with a Nikkor (Nikon, Japan) AF-S 24–120 mm f/4G ED VR lens, and mounted with different filters provided by MaxMax (LDP-LCC, Carlstadt, NJ, USA) was used. For the image calibration, a ColorChecker Passport Photo 2 (X-Rite, Grand Rapids, MI, USA) was used. The images were acquired in neutral mode to avoid all the enhancements provided by the camera's software (ver 1.0).

Since the replacement of photographic films, infrared false color and ultraviolet false color have become post-production techniques, elaborated through a graphic editor program.

In this study, NIR images were acquired with two different filters. The first image, called NIR 1, was acquired with a filter with full transmittance from 715 nm onwards, and the second image, NIR 2, using a filter with full transmittance starting from 850 nm onwards.

The combinations of filters mounted on the camera lens and the lamps used as the source of radiation are listed in Table 1.

Table 1. Combinations, for every technique, between radiation sources and filters mounted on the lens to obtain each photographic technique.

MBI Technique	Filter on Lens	Source of Radiation
UVR	XNite 330C	4× TL-D BLB 18W (Philips, Amsterdam, The Netherlands)
UVL	XNite CC1 + Zeiss T* UV	4× TL-D BLB 18W (Philips, The Netherlands)
VIS	XNite CC1	2× SuperLED 16W (6500 K) (Beghelli, Valsamoggia, Italy)
VIL	XNite 715 nm	2× SuperLED 16W (6500 K) (Beghelli, Italy)
NIR 1	XNite 715 nm	2× BR125 IR 150W (Philips, The Netherlands)
NIR 2	XNite 1000 nm	2× BR125 IR 150W (Philips, The Netherlands)

Images were acquired in *.NEF format, which contains low-processed data and allows entirely preserving the information recorded by the camera sensor when exported on graphic editor programs. The images after the elaboration were saved in *.TIF (tagged image file) format, with a resolution of 6529 × 4524 pixels at 24 bits.

2.3. Infrared Spectroscopy

ER FT-IR spectra were recorded using a portable Alpha spectrometer (Bruker Optics, Ettlingen, Germany) equipped with the external reflection module, operating in the range 7500–375 cm^{-1}. Spectra were acquired over an area of 3 or 5 mm (diameter of the probe head used) with 128 or 256 scans and a resolution of 4 cm^{-1}, depending on the characteristics of the surface under investigation. For instance, blue and brownish areas, which showed a more enhanced roughness of the surface, required the use of the 5 mm probe and the acquisition of 256 scans, to obtain a more satisfactory signal-to-noise ratio. The Kramers–Kronig algorithm was applied only in the 4000–375 cm^{-1} range to correct the derivative-like bands, while a general correction was avoided due to the variability of optical properties and morphological characteristics of the surface [33–35].

2.4. Raman Spectroscopy

Raman spectra were acquired with a portable Bravo Raman spectrometer (Bruker Optics, Ettlingen, Germany) with two laser excitations (DuoLaserTM), a technology (SSETM) to reduce fluorescence, a CCD detector, and laser power range < 100 mW. The measuring spot was 10–15 μm and the plastic head provided an original focal distance with the laser ideally focused when the instrument worked in contact [36–38].

2.5. Optical Microscopy

Images of the surface were taken with a portable microscope, Dino-Lite (Dino-Lite Europe, Almere, The Netherlands) 1,3 Mpixel with polarized light, to document the state of conservation, supporting the punctual analyses and highlighting the composition of the materials.

3. Results and Discussion

The combination of data obtained through the techniques described in Materials and Methods allowed for the identification of almost all the pigments used by the artist, and the mean thickness of the paint layers, increasing the knowledge of the technique used with this peculiar support. In Figure 3 all the measurement spots and map areas acquired are indicated.

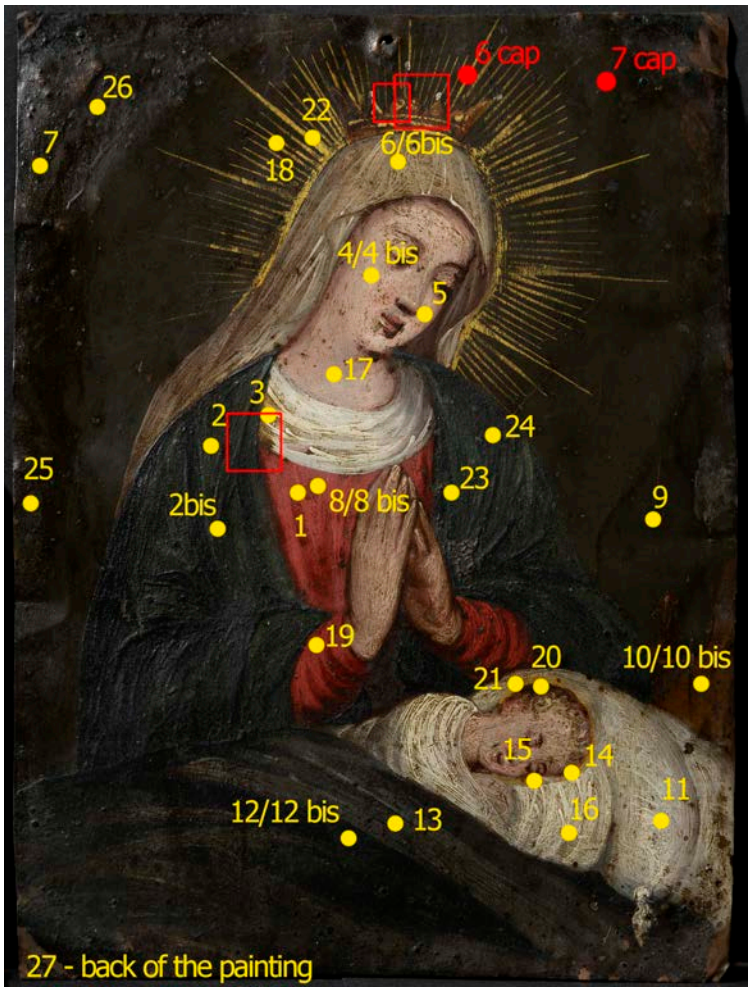

Figure 3. Image with the positions of the measurements. The capillary single spots and maps made with the Tornado are reported in red color (circle: single point, squared zones: maps). The XRF (custom instruments), Raman, and ER FT-IR measurement areas are reported in yellow.

3.1. Conservation Status

Observing the Virgin's mantle and the blanket on the bed, they seemed to be painted in a dark blue and in a grey color, respectively. Upon closer investigation, both surfaces appeared to have been achieved using a blue pigment. In particular, the mantle, in addition to the blue pigment, showed altered compounds ranging from green to brown, distinguishable under microscopic observation. On the contrary, the blanket showed only a thick brown layer containing many blue crystals (Figure 4).

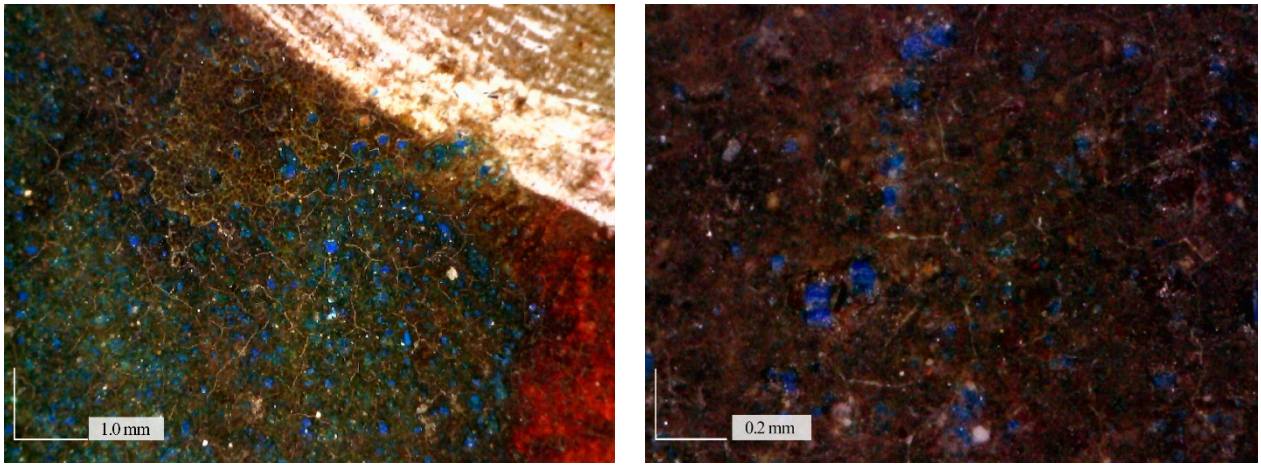

(**a**) (**b**)

Figure 4. Optical microscope details of (**a**) the mantle, magnification at 60×, and (**b**) the blanket, magnification at 220×.

The raking light image, besides the irregular surface, also showed the thickness of some painted areas such as the mantle and the pillow, as opposed to the thin background layer. Usually, in these types of paintings, the paint layer is very thin due to the surface characteristic of non-porous copper, although sometimes, more compact brushstrokes can be found, as in the case of draperies [2].

On the gap edges of these thick layers, such as the Virgin's vest, a white background was visible, but it did not seem to be equally distributed on the entire surface. For example, when observing the gaps on the gray background, only the copper was visible. This can suggest the use of a mixed technique, with some areas supported by a thicker layer of white background and other areas where the painter may have taken advantage of the copper's optical proprieties by using only the binding media or a very diluted paint [39].

The microscopic observation of the surface also showed a brown translucent material, more or less visible across the entire surface, especially in the painting hollows, which contained small dark particles trapped inside.

All these conservation issues made it difficult to quantify the real thickness of each layer. Thus, the thickness estimation given here shall be read as mean values. According to the XRF measurements and Monte Carlo simulations, all the zones were modelized as a three-layer zone: the painting layer, preparatory layer (lead white), and copper substrate. The brown translucent material was not considered in the model because of its inhomogeneous presence on the surface. The UVL image confirmed that, at least one previous restoration campaign had been performed on the artwork. The image showed the presence of an organic material on the edges, especially on the left and on the upper and lower sides. The substance did not appear on the folded corners, which indicates that its application on the surface certainly occurred before the damaging of the corners (Figure 5).

The hypothesis of the presence of this varnish as an original layer on the entire surface was excluded, due to the technique used for the painting. The use of copper as substrate, combined with an oil medium, immediately gave a shining aspect to the surface. The most likely scenario is that the varnish was applied on the entire surface, following a restoration procedure, and then partially removed, probably due to its degradation. Finally, the varnish could have been applied only on the edges to restore and prevent the falling of the painting layer. The UVL also excluded the presence of organic lakes, such as madder lake, which might have been used as a finish layer for the Virgin's robe, lips, or cheeks (Figure 5).

Figure 5. UVL image of the painting.

The ER FT-IR spectrum acquired on one of the luminescence areas confirmed the use of a varnish media. Although the spectrum was quite noisy, with the help of the reference spectra, it was possible to identify some absorption bands attributable to a dammar/mastic varnish [40–43]. The bands at 2950–2850 cm^{-1} (aliphatic CH stretching), 1710 cm^{-1} (C=O stretching), 1457 and 1382 cm^{-1} (CH_2 and CH_3 bending), and 1120 cm^{-1} (as C-O-C stretching) are perfectly in agreement with the presence of a dammar/mastic varnish.

Unfortunately, the painting came from an antique market and no certain information was available on its conservation history.

3.2. Metallic Support and Preparation Layer

The XRF analyses on the back of the copper plate showed the presence of pure copper, with a few minor elements such as calcium, iron, lead, and sulfur. This was consistent with the analyses of other paintings on copper [44] where the high quality of the plate reflected the carefulness of the craftsman and the high level of technical development to create thin metal plates.

The analyses acquired on the painted surface showed the presence of lead in each measure. The ubiquity of the lead suggested the use of a ground layer formed by lead white and oil as described in the literature [10,45] to isolate the paint layer from the copper substrate, avoiding corrosion phenomena.

To try to identify the aged binding medium of the painting, the red area (the Virgin's vest) was chosen, because of the characteristics of vermilion, identified in the Raman and XRF spectra, which does not absorb IR radiation in the MIR range and does not induce the formation of detectable products through interaction with the binder, providing a spectrum closely similar to an unpigmented layer of binding medium [46].

The spectrum showed two bands at 4335 and 4260 cm^{-1} attributable to the combination bands of stretching and bending of the methylene group [42,47]. Although with low intensity, the bands due to the methylene group (CH_2) stretching were visible in the

range 2950–2850 cm^{-1}. The band at 1740 cm^{-1} was attributable to the stretching of a carbonyl group in an ester [34]. All these data agreed with the presence of a siccative oil as a binding medium.

The spectrum also showed small bands at 1620 and 1324 cm^{-1} due to the presence of calcium oxalate and at 1420 and 670 cm^{-1} attributable to lead white [40–43].

The presence of a white preparation layer would have been expected to enhance the presence of preliminary drawing, especially if it was made with charcoal; nonetheless, both near-infrared images, up to 720 nm and 850 nm, did not show any preliminary drawing.

3.3. Pigments

A first indication of the pigments used in the painting was provided by the study of near-infrared reflected false color (IRFC) and ultraviolet false color (UVFC). With both techniques, it was possible to recognize the use of vermilion for the Virgin's vest and for the lips (yellow/orange in the IRFC image). In the IRFC image, the skin appeared with a slight yellow hue suggesting the use of vermilion as a red component. The presence of a dark color on the Virgin's mantle implies the probable use of Azurite as a blue pigment. The UVFC observations were in accordance with what was revealed by IRFC (Figure 6).

(**a**) (**b**)

Figure 6. (**a**) IRFC; and (**b**) UVFC of the painting.

3.3.1. Flesh Tones

Flesh tones were obtained with a mixture of vermilion and lead white as suggested by the XRF spectrum where mercury and lead were the main elements present. In particular, the lead counts were higher than in the background, suggesting the use of lead white also as a white pigment in the paint layer (see Figure 7). The Raman spectrum showed the presence of vermilion with a strong band at 255 cm^{-1} and bands at 285 and 345 cm^{-1} in accordance with the literature [46]. A band at 1052 cm^{-1}, attributable to the $\nu(CO_3^{2-})$ of lead white, was also detected (Figure 8). The ER FT-IR spectrum, instead, showed only bands that could be assigned to lead white.

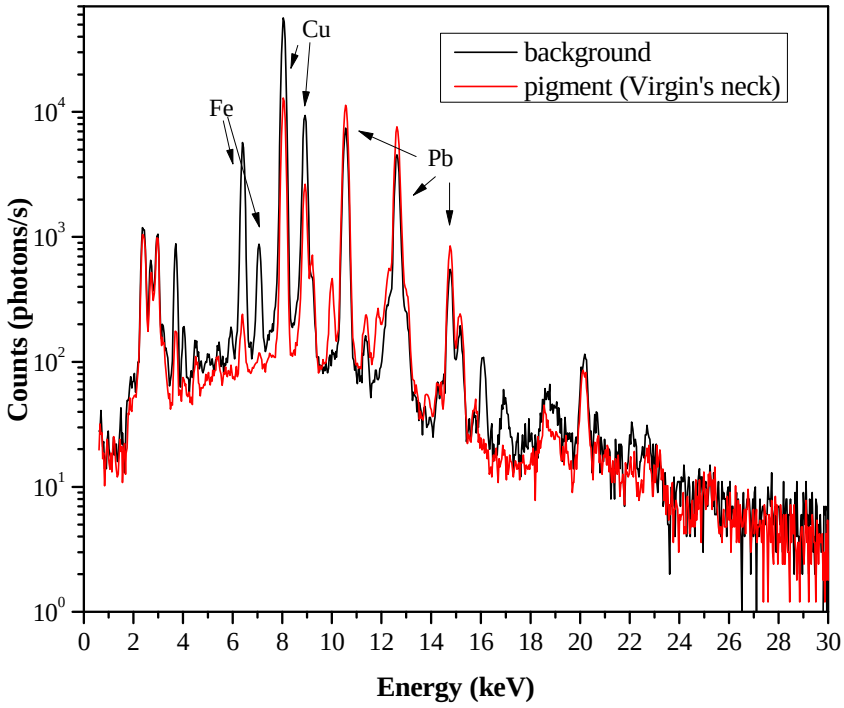

Figure 7. XRF spectrum of a flesh tone (Virgin's neck) compared to the background. The background exhibits higher iron and copper contents, whereas the pigment shows a higher lead concentration.

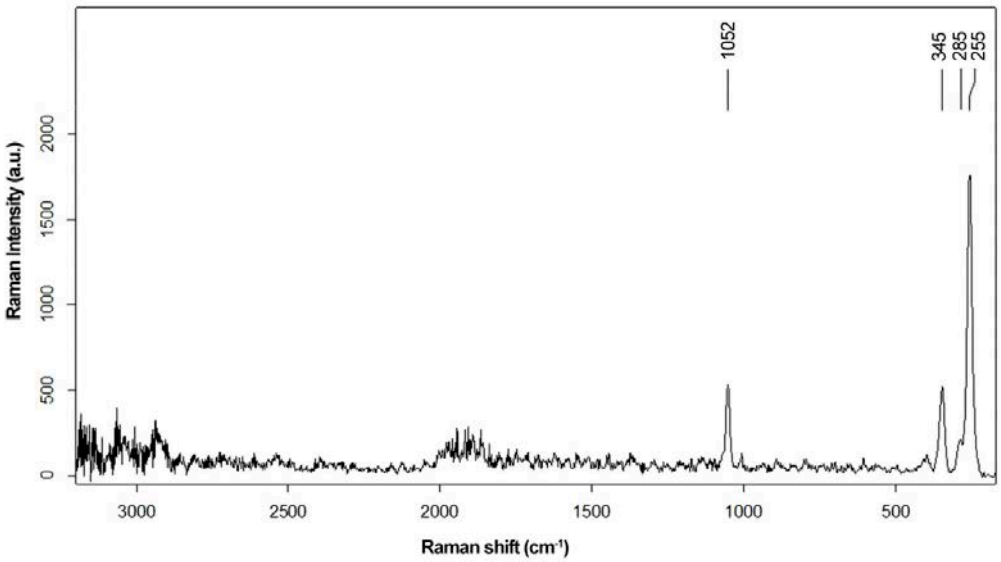

Figure 8. Raman spectrum of an area on the Virgin's neck.

The case of both of the cheeks was different, where two retouched areas were highlighted in the MBI images and documented by the microscope. The XRF measurements coupled with Monte Carlo simulations on these retouched areas showed the presence of titanium, iron, and copper as the main constituents, while mercury and lead were completely absent (see Figure 9). Moreover, the lead content in the preparation layer was lower than in other areas. This confirms the presence of some retouching using titanium white (TiO_2) and iron oxide (Fe_2O_3), with the removal of almost all of the preparation layer. The thickness of the layers, with a very low density indeed, was, respectively, 420 µm for the painting layer and 10 µm for the preparation layer.

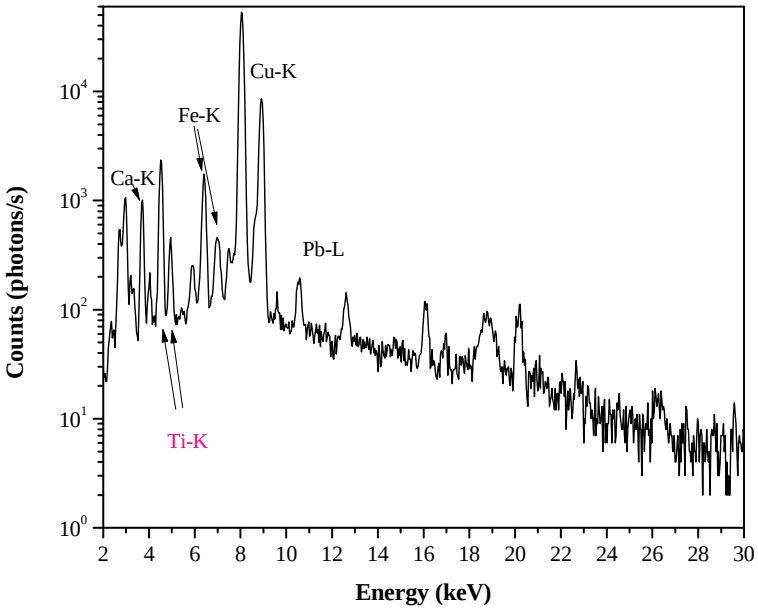

Figure 9. X-ray spectrum of the Virgin's cheek displaying several peaks, notably indicating the presence of titanium (in red).

3.3.2. Red

XRF analyses were acquired in several areas of the red vest, some in fully red and some in dark red areas. The measurements were intended to clarify if a difference in hue followed a difference in composition.

Figure 10a,b show two XRF spectra and the corresponding spectra obtained with a Monte Carlo simulation, acquired in two different red areas.

Qualitatively, both spectra had the same composition, mainly vermillion, but data obtained by the Monte Carlo simulations showed that, in the outer layer, the copper was practically absent in the red area while it had a 3% relative concentration in the dark red area. More important, mercury was almost 50% higher in the red area (37%) compared to the darker one (26%). The estimated thickness of the red layer was 410 μm while it decreased to 260 μm in the darker part. At first glance, the thickness of these layers can appear too high, but it can be explained by thicker brush strokes and a probably large content of voids (represented by oxygen in the Monte Carlo model of the red layer), and light elements (sulfur and binder material).

XRF and Raman spectra confirmed that vermillion was used to paint the red areas, as suggested by IRFC [46]. The ER FT-IR spectrum, as reported before, showed only peaks related to the presence of calcium oxalates and a possible siccative oil.

3.3.3. White

XRF measurements, with a Monte Carlo simulation, were performed in several areas, such as the veil and the pillow. The elements detected in the white pigment were lead (35%), copper (1.5%, probably due to a migration from the metallic support to the surface), iron (0.15%), and titanium (0.15%), plus other elements in traces. Its mean thickness was 50 μm. The preparation layer was always about 10 μm.

The ER FT-IR spectrum of the white area on the pillow showed the typical absorption bands due to the presence of lead white. Applying the KK algorithm at the MIR region of the spectrum, the bands at 1415 (as CO_3^{2-} stretching) and 683 cm^{-1} (CO_3^{2-} bending), attributable to lead white, became clearly detectable [46,47].

Besides the bands at 4328 and 4270 cm^{-1} (combination bands of methylenic C-H stretching and bending), 2950–2850 cm^{-1} (C-H stretching), and 1749 cm^{-1} (C=O stretching) due to the aged siccative oil, the spectrum showed the presence of a little amount of calcium oxalates (bands at 1650 and 1330 cm^{-1}) [40–43].

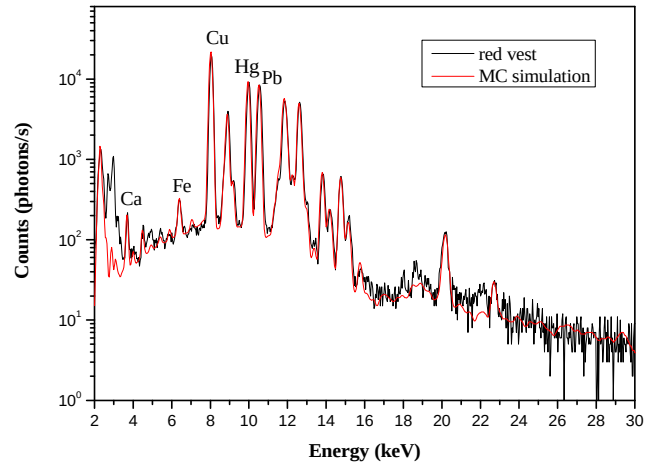

(**a**)

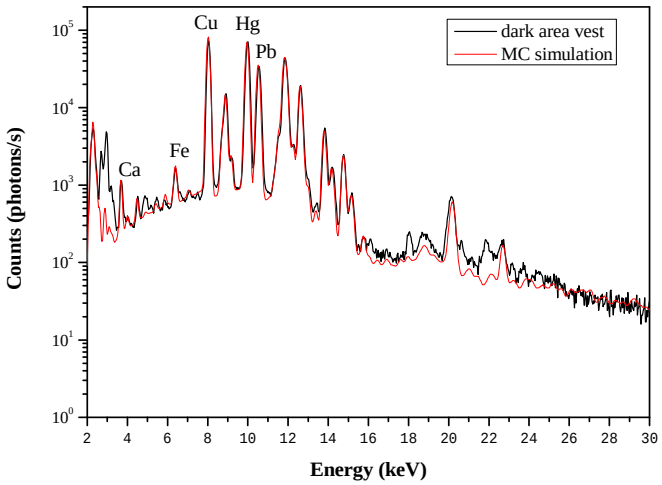

(**b**)

Figure 10. (**a**) XRF spectrum corresponding to the area with a red color in the Virgin's vest and MC simulation; (**b**) XRF spectrum of an area with a darker red color in the Virgin's vest and MC simulation. In the latter, the Hg concentration is higher than in Figure (**a**), as evidenced by the comparison between the Hg peak and the Pb peak.

The Raman spectrum, recorded on the same point, confirmed the presence of lead white [48] and the presence of a small amount of carbon black, as suggested by the broad bands at 1585 and 1300 cm^{-1}. The presence of a broad peak at 2900 cm^{-1} was probably attributable to the C-H vibrations of a non-identified organic material [49].

The ER FT-IR spectrum of the Virgin's veil appeared quite similar to the other white areas analyzed. The Raman spectrum of the veil showed the peak for lead white and a small amount of vermilion (259 cm^{-1}) and goethite (389 cm^{-1}) [40–43].

3.3.4. Brown

The only brown areas not attributed to degradation processes were those of the headboard and the crown. MBI techniques, on the headboard, suggested the presence of an earth pigment such as ocher and a vermilion for the red decorations. Observation, by means of the portable microscope, of the area showed the presence of small red particles mixed with a yellow-brownish color beside the decoration details painted in red. ER FT-IR analysis allowed to identify lead white, goethite (α–Fe(O)OH, 904, 795 and 400 cm^{-1}), hematite

(α–Fe_2O_3, 570 and 475 cm^{-1}), and calcium oxalate. Very small bands at 3695, 3620, 1120, 1040, 550, and 470 cm^{-1} suggested the presence of a small amount of an aluminosilicate, kaolinite [50].

The Raman spectrum showed, in addition to the peaks due to vermilion, a peak at 388 cm^{-1} and a shoulder at 295 cm^{-1}, which are characteristics of goethite [51,52]. Some small signals attributable to hematite were also detected.

Monte Carlo simulations showed that the brown headboard was formed by a 100 µm thick layer composed of copper (40%), lead (13%), iron (8%), calcium (5.5%), mercury (2%), chloride (5%), and sulfur (3%). The presence of lead, iron, and mercury was in accordance with the results obtained from the ER FT-IR, as well as calcium, while chloride and sulfur suggested the presence of superficial compounds related to air pollution.

The other brown area, the crown, was investigated with XRF mapping and a polycapillary lens due to its small size. The maps of each element showed the presence of copper on almost the entire surface, except for the area where lead was detected, and the copper signal suffered from the attenuation effect, due to the presence of lead atoms in the upper layer. Iron and mercury were visible in the brown areas, confirming that the brown color was obtained by mixing ochers and vermilion (Figure 11).

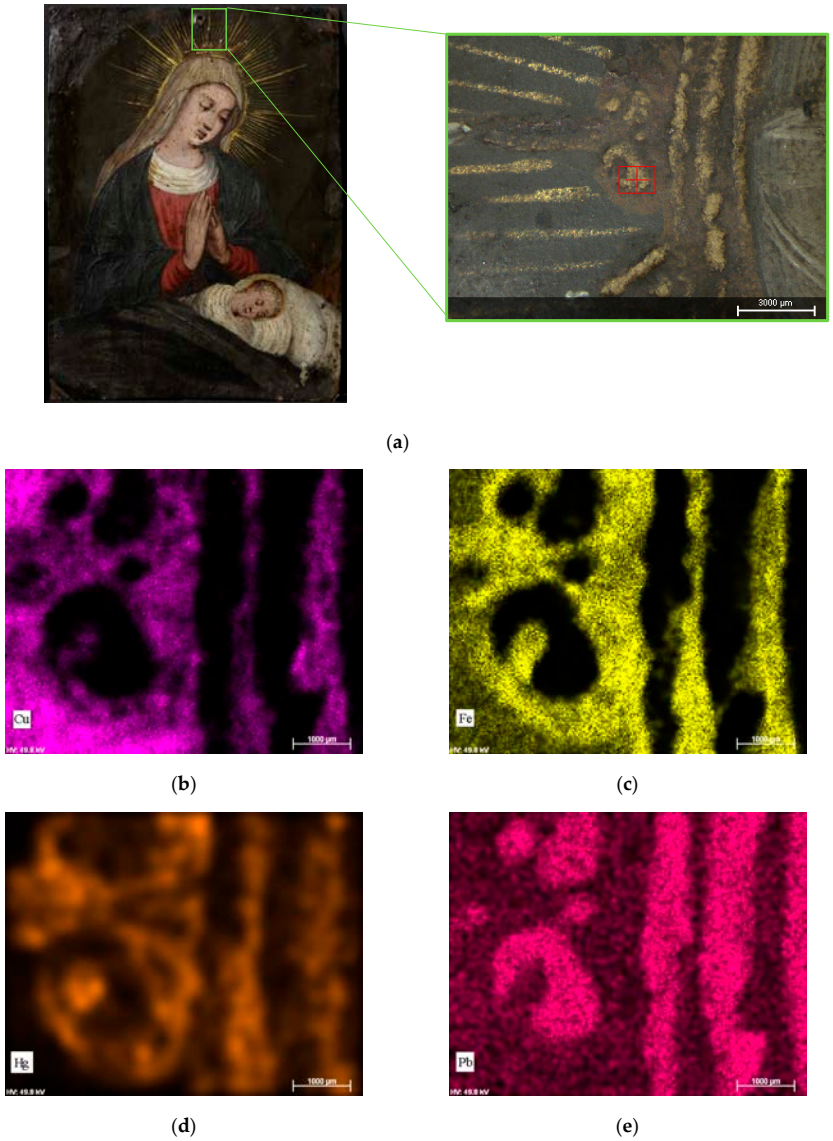

Figure 11. (**a**) Visible image with the indication of the area analyzed in green and detail of the area to 50× of magnification; (**b**) map of copper; (**c**) map of iron; (**d**) map of mercury; (**e**) map of lead.

In the light yellow area, the micro XRF analysis indicated the presence of a small amount of tin combined with the lead which suggested the use of a lead-tin yellow [53] (Figure 12).

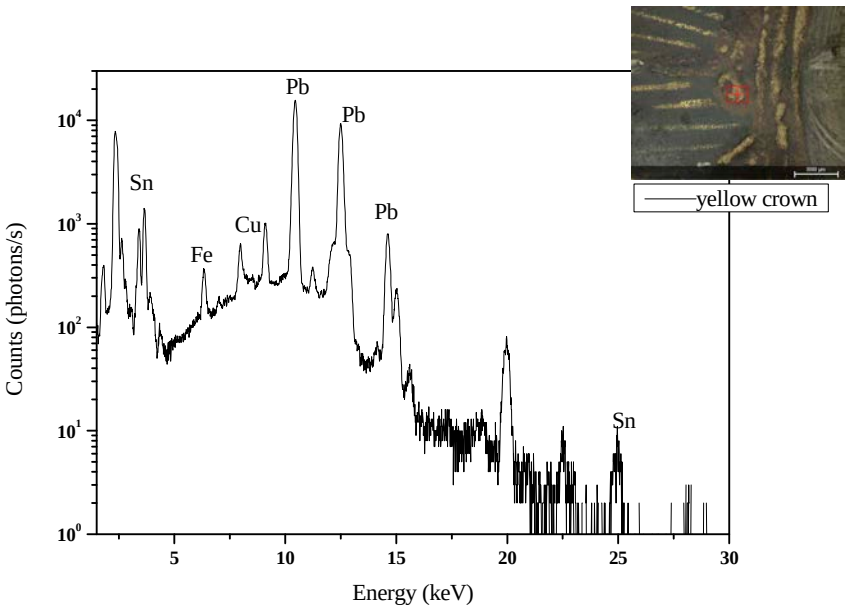

Figure 12. XRF spectrum with a polycapillary lens of the yellow decoration on the crown.

3.3.5. Gold

The XRF analysis on both aureoles, the Child and the Virgin, showed the presence of gold. In this case, close observation through the microscope suggested the use of shell gold or powder gold, as shown in Figure 13.

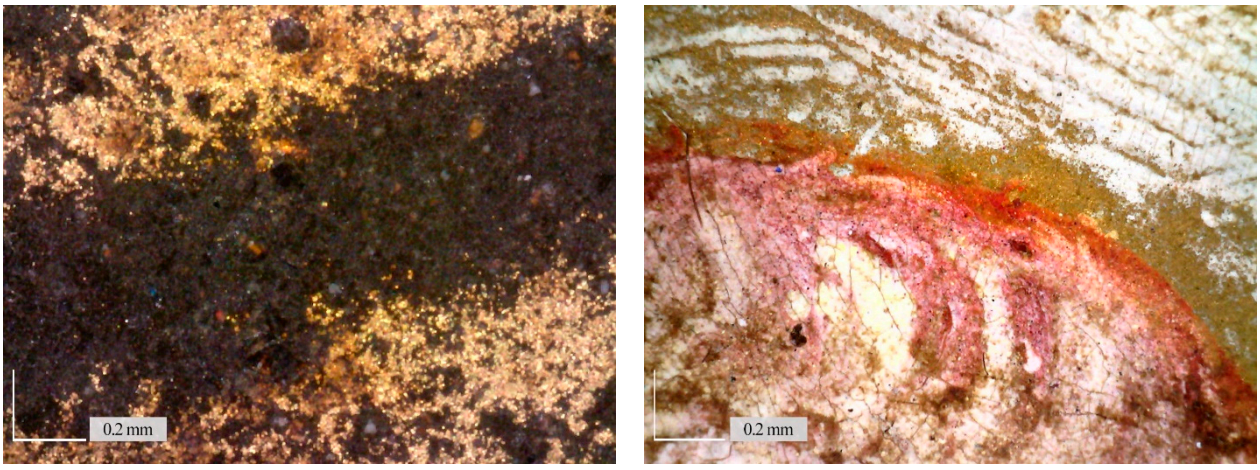

(**a**) (**b**)

Figure 13. Detail at high magnification of (**a**) the Virgin aureole, magnification at 220×; (**b**) detail of the Child's aureole, magnification at 220×.

Observing the Child's head, it was also possible to identify some areas where the gold was painted over the red outline of the head, suggesting the application of gold as the last refinement (Figure 13). However, the dimension of the gold parts was comparable or smaller than the X-ray measurement spot size, and so they may include information from surrounding areas. For this reason, the Monte Carlo simulation was not applied.

μXRF was used to map the area corresponding to the rays on the left of the Virgin's aureole (Figure 14). The maps for each single element showed the presence of gold in the

rays. In addition, the presence of a lead-white-based background and the presence of iron on the entire brown-grey background was also confirmed, suggesting the use of a very diluted paint for this area.

(**a**)

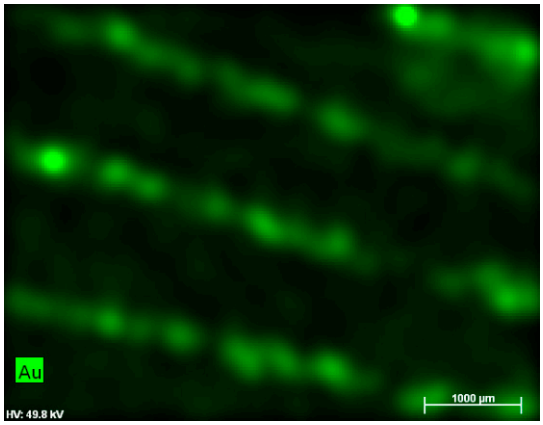

(**b**)

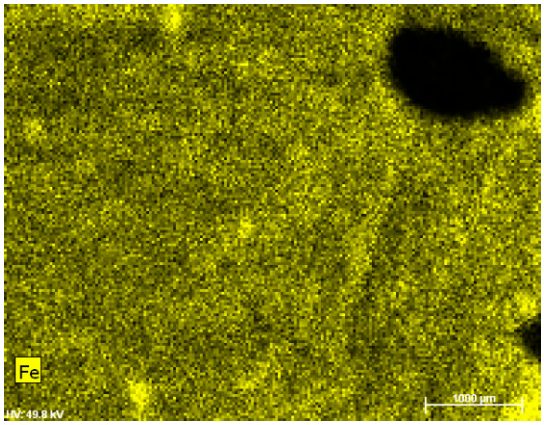

(**c**)

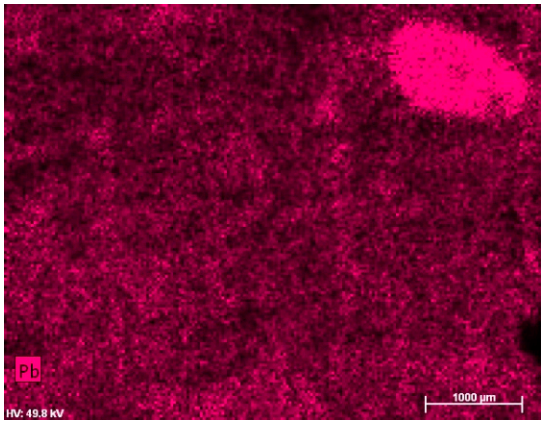

(**d**)

Figure 14. (**a**) Visible image with the indication of the area analyzed in green and detail of the area at 50× magnification; (**b**) map of the concentration of gold; (**c**) map of the concentration of iron; (**d**) map of the concentration of lead.

3.3.6. Blue and Dark Areas

Unfortunately, the blue pigment used for the mantle was very degraded. Observation at high magnification showed the presence of a base with blue crystals and at least two layers of degradation products, one green and the other brown, as visible in Figure 15.

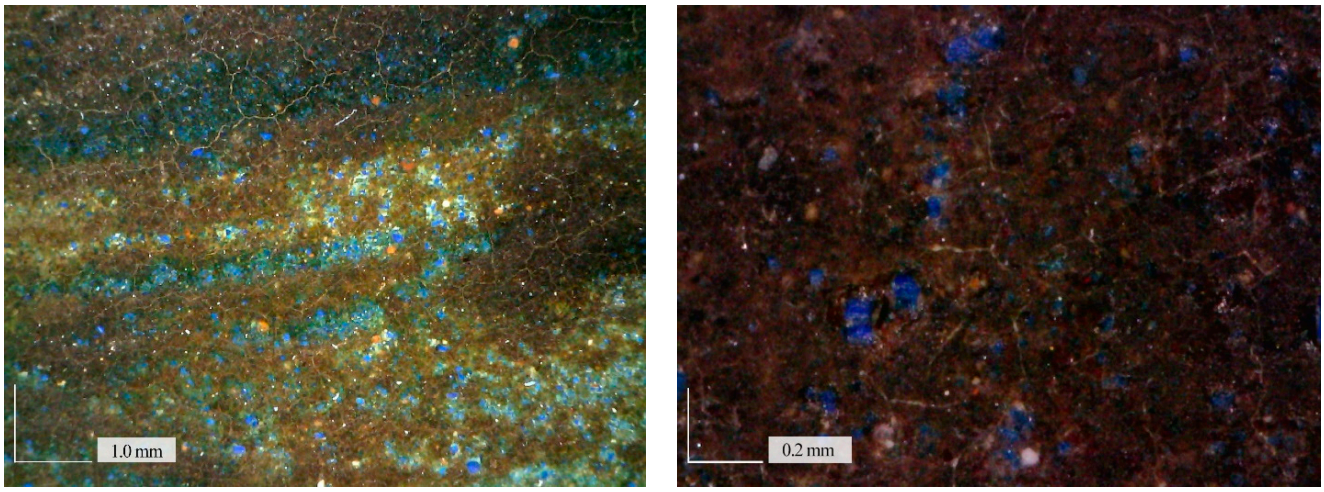

(**a**) (**b**)

Figure 15. Two details of the degradation visible on the blue surface (**a**) Virgin's mantle with green and brown degradation products, at 60× magnification; (**b**) the blanket with a thick layer of brown material on the top, at 220× magnification.

Several areas were analyzed by ER FT-IR, but all the spectra presented a low S/N ratio, caused by the rough surface, that disguised the main peaks useful for the characterization of the materials. Despite this, the technique enhanced the combination and overtone bands, which have been used for characterization. The second overtone of CO_3^{2-} stretching at 4376 cm^{-1}, the combination band of stretching and scissoring of O-H at 4244 cm^{-1}, the OH stretching at 3435 cm^{-1}, and the CO_3^{2-} asymmetric stretching at about 1435 cm^{-1} allowed to confirm the presence of azurite [54,55]. The ER FT-IR spectra also showed small bands attributable to low amounts of calcium oxalate, kaolinite, lead white, and calcite (Figure 16).

Raman spectra showed only a small peak corresponding to lead white, which confirmed the presence of this pigment in a mixture with the original blue paint.

Observing some of the images at high magnification, spotted particles of black materials embedded in the superficial brownish layer were visible. The presence of this material could be related to the residual combustion from candles or oil for lamps.

XRF was performed on both of the Virgin's shoulders' blue areas. Even in this case, the optical microimages showed a very irregular surface with strong alterations or absence of the pictorial layer.

With all the limitations listed above, XRF measurements and a Monte Carlo simulation were performed.

Of course, the results must be considered as mean values, even for the same spot. The mantle color was mainly formed by elements such as lead (40%) and copper (23%), with calcium (4.7%) and iron (2.3%). Sulfur was also detected (6.2%), probably due to the deposition of air pollution from the environment. Its thickness was 50 μm, considerably thinner than the red areas.

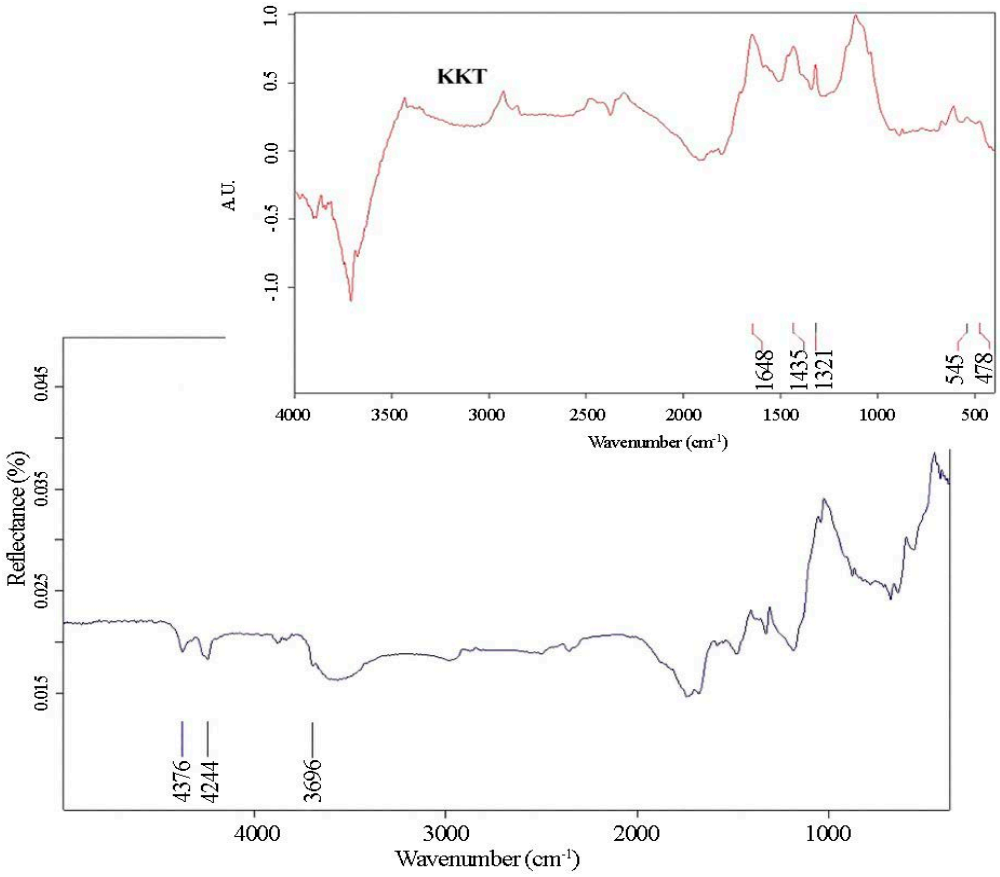

Figure 16. ER FT-IR spectrum of a measure on the mantle, in blue, and the correspondence KK transformation spectrum in red.

Another area, which was originally blue, was the blanket on the bed. Observations at high magnification showed the presence of small crystals of blue, almost completely covered by a thick layer of unidentified material, with two different brown hues.

As was the case of the red area, the light-colored part appeared to have been applied on the darker one. The light part was estimated, by Monte Carlo simulation, to be 130 µm thick while the darker was 80 µm thick. The composition of both areas was quite similar, but the light part showed higher lead contents (35% instead of 30%), and lower calcium (0.30% against 0.60%), and iron (0.17% against 0.40%).

Some attempts to recognize the degraded materials on the surface were made without any results.

3.3.7. Grayish-Brown Background

The background of the painting was not a well-defined color; it showed a grayish hue but with a brown shade. Even the observations under the microscope did not allow a better definition of the color. Some hypotheses were made regarding the appearance of the background which did not fit the expected color, considering the data obtained from the analyses. One of these involved the presence of a degradation process, not well-identified with the methodologies applied, which changed the final appearance of the paint layer.

The XRF analyses showed the presence of Cu (27%), Fe (7.3%), Pb (26%), and traces of Mn (0.05%) (Figure 17). Regarding the thicknesses, the painting layer was 27 µm-thick while the lead white substrate was 5 µm thick.

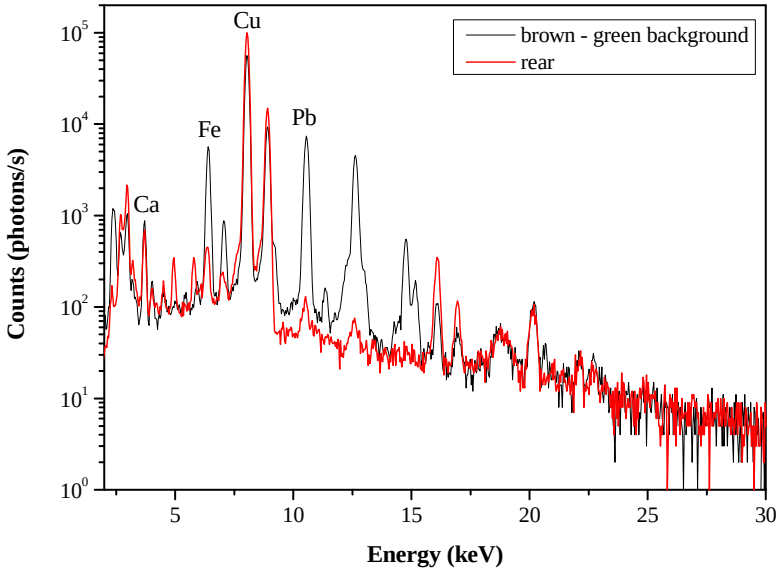

Figure 17. XRF spectrum of the brown-green background compared with the XRF spectrum of the rear.

The presence of iron and traces of manganese suggested the presence of an earth pigment (Figure 14) and this hypothesis was confirmed by ER FT-IR.

Indeed, the IR spectra acquired on the background, as well as lead white and a large amount of calcium oxalate, clearly showed the presence of goethite (α-Fe(O)OH, 900, 792 and 409 cm^{-1}), of a small amount of hematite (α-Fe_2O_3, 570 and 473 cm^{-1}), and, probably, of manganese dioxide (MnO_2, in the range 600–400 cm^{-1} overlapping that of hematite), the usual main components of a natural earth umber earth (Figure 18).

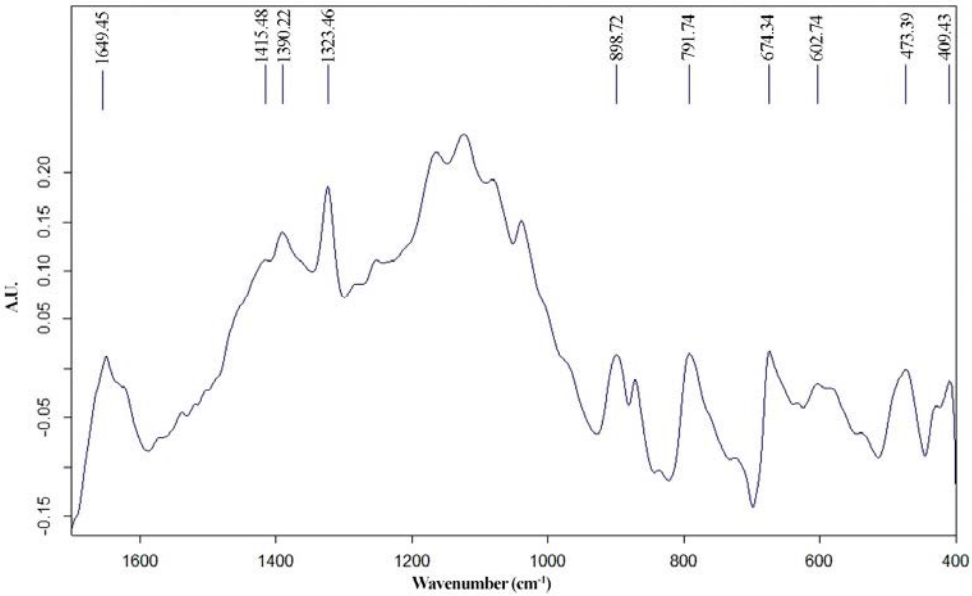

Figure 18. Detail from 1700 to 400 cm^{-1} of KKT of spectrum on the grey-brownish background.

However, only further analyses could help in the attempt to identify with certainty the pigment or the mixture used for the background, or the degradation materials produced which have resulted in this undefined color.

Table 2 summarizes the results obtained with the Monte Carlo simulation for each color analyzed.

Table 2. The thickness of each layer on measured points expressed as micrometers. The error estimation is about 10%.

Spot	Painting Layer (μm)	Prep. Layer (μm)	Copper Subst. (μm)
Dark blue on the blanket	80	10	600
Light blue on the blanket	130	10	600
Brownish-gray background	27	5	600
Blue, Virgin's mantle	50	10	600
Brown, headboard	100	10	600
Light red, Virgin's vest, chest	410	10	600
Dark red, Virgin's red vest, chest,	260	10	600
Virgin's veil	180	10	600
Flesh tone	420	10	600
White pillow	50	10	600

The error in the thickness estimation was about 10% of the reported one. The 10% variance stemmed from the minimum noticeable difference in the background levels observed when comparing the experimental and measured spectra.

4. Conclusions

The paper analyzed a small painting from a private collection whose distinguishing feature is the copper plate used as a support. The use of this metal support found its popularity in the 16th century, especially for small formats and with subjects such as religious images. In this case, the subject of the painting is the Virgin contemplating the sleeping Child, widely spread during the XVII century.

The first-time use of Monte Carlo simulations on this type of artefact allowed us to estimate the average thickness and composition of the different layers, including the thin layer of lead white used as the preparation layer. The simulations suggested that the thickest layers were the red areas, in particular the bright red layer, while the other paint layers roughly had an average thickness of 80 μm, except for the background color, which was the thinnest layer. This technique, as part of a multimethodological approach, was integrated with other nondestructive techniques: multiband imaging, Raman and ER FT-IR spectroscopy, and optical microscopy.

This multimethodological approach allowed us to recognize almost all the pigments used by the artist. The major difficulties in the characterization of the materials arose from the origin of the painting, made by an anonymous painter, and the lack of information on its conservation history and possible subsequent interventions.

Nevertheless, the analyses showed the presence of a siccative oil as a binding medium and the use of a color palette in which all the identified pigments (azurite, vermilion, lead white, ochers, and gold) agreed with the supposed period of production of the artwork.

The analyses also led to the characterization of some retouches, obtained with a mixture of titanium white and red ochers. UV luminescence and ER FT-IR spectroscopy highlighted the presence of a dammar/mastic varnish, probably applied during previous restoration work, and of degradation and pollution materials such as calcium oxalates (decomposition of organic products) and carbon particles (probably due to the exposure to burning candles).

Some questions remain uncertain, such as the color in the background, but the paper aimed to identify the materials while completely avoiding sampling from this fragile and unique artefact, and the results obtained will extend the knowledge of these peculiar works of art.

Author Contributions: Conceptualization, R.I. and A.B.; investigation, R.I., A.P., L.M. and A.B.; resources, R.I., A.P. and A.B.; data curation, A.B.; writing—original draft preparation, R.I., A.P. and A.B.; writing—review and editing, R.I., G.B. and A.B.; visualization, R.I. and G.B.; supervision, A.B.; funding acquisition, R.I. and A.B. All authors have read and agreed to the published version of the manuscript.

Funding: This research was funded by Programma Operativo Nazionale (PON) Ricerca e Innovazione 2014–2020—Asse I "Capitale umano", Azione I.2 A.I.M, "Attrazione e Mobilità Internazionale dei Ricercatori", D.D. del MIUR n. 407 del 27 febbraio 2018—Linea 2 "Attrazione" [AIM1843180-3—CUP J54I18000380001] (R.I.) and FAR 2020 (R.I. and A.B.).

Data Availability Statement: The data presented in this study are available on request from the corresponding author.

Acknowledgments: The authors are grateful to CIRTEBEC—Centro Interuniversitario di Ricerca sulle Tecnologie per i Beni Culturali—GAUSS Laboratories of the Università degli Studi di Sassari with the support of Regione Autonoma della Sardegna, for providing equipment.

Conflicts of Interest: The authors declare no conflicts of interest.

References

1. Komanecky, M.K.; Horovitz, I.; Eastaugh, N. Antwerp artists and the practice of painting on copper. *Stud. Conserv.* **1998**, *43*, 136–139. [CrossRef]
2. Terenzi, M.G.; Ferrucci, F.; Amadori, M.L. *Dipinti su Rame: Storia, Tecnica, Fenomeni di Degrado, Diagnostica; Indicazioni per la Conservazione e il Restauro*; Collana Il: Padova, Italy, 2006.
3. Maetzke, A.M. (Ed.) *Piero della Francesca*; L'opera, Monografie: Silvana, Milan, 2013.
4. Madonna col Bambino e Santi, Angeli e Federico da Montefeltro (Pala di San Bernardino), Pinacoteca di Brera. Available online: https://pinacotecabrera.org/collezione-online/opere/vergine-con-il-bambino-angeli-e-santi-pala-montefeltro/ (accessed on 30 September 2023).
5. Scotti, R. *Barocco Andino. Arcangeli Guerrieri, Madonne e Dee, Santi Meticci*; Ananke: Torino, Italy, 2009.
6. Mauquoy-Hendrickx, M. *Les Estampes des Wierix: Conservées au Cabinet des Estampes de la Bibliothèque Royale Albert Ier: Catalogue Raisonné Enrichi de Notes Prises dans Diverses Autres Collections*; Bibliothèque Royale Albert Ier: Bruxelles, Belgium, 1983.
7. Van Ruyven-Zeman, Z.; Leesberg, M. *The Wierix Family*; Sound & Vision Publishers: Ouderkerk aan den Ijssel, The Netherlands, 2004; Available online: https://books.google.it/books?id=-frkAAAAMAAJ (accessed on 30 September 2023).
8. British Museum. Hieronymus Wierix. Available online: https://www.britishmuseum.org/collection/object/P_1859-0709-3031 (accessed on 30 September 2023).
9. Sacristán-Ramírez, C. Audible Paintings: Religious Music and Devotion to the Infancy of Christ in the Art of the Viceroyalty of Peru. *MAVCOR J.* **2019**, *3*. [CrossRef]
10. Horovitz, I. Paintings on copper supports: Techniques, deterioration and conservation. *Conservator* **1986**, *10*, 44–48. [CrossRef]
11. Sherman, J. The theoretical derivation of fluorescent X-ray intensities from mixtures. *Spectrochim. Acta* **1955**, *7*, 283–306. [CrossRef]
12. Shiraiwa, T.; Fujino, N. Theoretical Calculation of Fluorescent X-ray Intensities in Fluorescent X-ray Spectrochemical Analysis. *Jpn. J. Appl. Phys.* **1966**, *5*, 886. [CrossRef]
13. Mantler, M. X-ray fluorescence analysis of multiple-layer films. *Anal. Chim. Acta* **1986**, *188*, 25–35. [CrossRef]
14. De Boer, D.K.G. Calculation of X-ray fluorescence intensities from bulk and multilayer samples. *X-ray Spectrom.* **1990**, *19*, 145–154. [CrossRef]
15. Cesareo, R.; Buccolieri, G.; Castellano, A.; Lopes, R.T.; De Assis, J.T.; Ridolfi, S.; Brunetti, A.; Bustamante, A. The structure of two-layered objects reconstructed using EDXRF-analysis and internal X-ray ratios. *X-ray Spectrom.* **2015**, *44*, 233–238. [CrossRef]
16. Cesareo, R.; Brunetti, A. Metal sheets thickness determined by energy-dispersive X-ray fluorescence analysis. *J. X-ray Sci. Technol.* **2008**, *16*, 119–130.
17. Cesareo, R. Gold, gildings, and tumbaga from the Moche tomb of the Lady of Cao: An EDXRF test for the internal ratio method. *X-ray Spectrom.* **2019**, *48*, 202–207. [CrossRef]
18. Trojek, T.; Wegrzynek, D. X-ray fluorescence Kα/Kβ ratios for a layered specimen: Comparison of measurements and Monte Carlo calculations with the MCNPX code. *Nucl. Instrum. Methods Phys. Res. Sect. A Accel. Spectrometers Detect. Assoc. Equip.* **2010**, *619*, 311–315. [CrossRef]
19. Pessanha, S.; Manso, M.; Antunes, V.; Carvalho, M.L.; Sampaio, J.M. Monte Carlo simulation of portable X-ray fluorescence setup: Non-invasive determination of gold leaf thickness in indo-Portuguese panel paintings. *Spectrochim. Acta Part B At. Spectrosc.* **2019**, *156*, 1–6. [CrossRef]
20. Bottigli, U.; Brunetti, A.; Golosio, B.; Oliva, P.; Stumbo, S.; Vincze, L.; Randaccio, P.; Bleuet, P.; Simionovici, A.; Somogyi, A. Voxel-based Monte Carlo simulation of X-ray imaging and spectroscopy experiments. *Spectrochim. Acta Part B At. Spectrosc.* **2004**, *59*, 1747–1754. [CrossRef]

21. Golosio, B.; Schoonjans, T.; Brunetti, A.; Oliva, P.; Masala, G.L. Monte Carlo simulation of X-ray imaging and spectroscopy experiments using quadric geometry and variance reduction techniques. *Comput. Phys. Commun.* **2014**, *185*, 1044–1052. [CrossRef]
22. Brunetti, A.; Sanchez Del Rio, M.; Golosio, B.; Simionovici, A.; Somogyi, A. A library for X-ray–matter interaction cross sections for X-ray fluorescence applications. *Spectrochim. Acta Part B At. Spectrosc.* **2004**, *59*, 1725–1731. [CrossRef]
23. Schoonjans, T.; Brunetti, A.; Golosio, B.; Del Rio, M.S.; Solé, V.A.; Ferrero, C.; Vincze, L. The xraylib library for X-ray-matter interactions. Recent developments. *Spectrochim. Acta Part B At. Spectrosc.* **2011**, *66*, 776–784. [CrossRef]
24. Brunetti, A.; Golosio, B.; Schoonjans, T.; Oliva, P. Use of Monte Carlo simulations for Cultural Heritage X-ray fluorescence analysis. *Spectrochim. Acta Part B At. Spectrosc.* **2015**, *108*, 15–20. [CrossRef]
25. Van Grieken, R.; Markowicz, A. (Eds.) *Handbook of X-ray Spectrometry*; Practical Spectroscopy Series; CRC Press: Boca Raton, FL, USA, 2001; Volume 29.
26. Brunetti, A.; Steger, T.J. X-ray spectra background fitting by projection onto convex sets. *Nucl. Instrum. Methods Phys. Res. Sect. A Accel. Spectrometers Detect. Assoc. Equip.* **2000**, *441*, 504–509. [CrossRef]
27. Steenstrup, S. A simple procedure for fitting a background to a certain class of measured spectra. *J. Appl. Crystallogr.* **1981**, *14*, 226–229. [CrossRef]
28. Greenberg, D.; Steinhauser, S. *Integrating Imaging and Analytical Technologies for Conservation Practice*; The Getty Conservation Institute: Los Angeles, CA, USA, 2013.
29. Cosentino, A. Identification of pigments by multispectral imaging; a flowchart method. *Herit. Sci.* **2014**, *2*, 8. [CrossRef]
30. Jones, C.; Duffy, C.; Gibson, A.; Terras, M. Understanding multispectral imaging of cultural heritage: Determining best practice in MSI analysis of historical artefacts. *J. Cult. Herit.* **2020**, *45*, 339–350. [CrossRef]
31. Dyer, J.; Verri, G.; Cupitt, J. *Multispectral Imaging in Reflectance and Photo-Induced Luminescence modes: A User Manual*; The British Museum: London, UK, 2013.
32. Webb, E.K.; Robson, S.; MacDonald, L.; Garside, D.; Evans, R. Spectral and 3D cultural heritage documentation using a modified camera. *Int. Arch. Photogramm. Remote Sens. Spat. Inf. Sci. ISPRS Arch.* **2018**, *42*, 1183–1190. [CrossRef]
33. Derrik, M.R.; Stulik, D.; Landy, J.M. *Infrared Spectroscopy in Conservation Science*; The Getty Conservation Institute: Los Angeles, CA, USA, 1983. [CrossRef]
34. Meilunas, R.J.; Bentsen, J.G.; Steinberg, A. Analysis of aged paint binders by ftir spectroscopy. *Stud. Conserv.* **1990**, *35*, 33–51. [CrossRef]
35. Rosi, F.; Cartechini, L.; Monico, L.; Gabrieli, F.; Vagnini, M.; Buti, D.; Doherty, B.; Anselmi, C.; Brunetti, B.G.; Miliani, C. *Tracking Metal Oxalates and Carboxylates on Painting Surfaces by Non-Invasive Reflection Mid-FTIR Spectroscopy*; Metal Soap in Art. Cultural Heritage Science; Springer: Cham, Switzerland, 2019; pp. 173–193. [CrossRef]
36. Smith, G.D.; Clark, R.J.H. Raman microscopy in archaeological science. *J. Archaeol. Sci.* **2004**, *31*, 1137–1160. [CrossRef]
37. Jehlička, J.; Culka, A.; Bersani, D.; Vandenabeele, P. Comparison of seven portable Raman spectrometers: Beryl as a case study. *J. Raman Spectrosc.* **2017**, *48*, 1289–1299. [CrossRef]
38. Innocenti, S.; Balbas, D.Q.; Pezzati, L.; Fontana, R.; Striova, J. Portable Sequentially Shifted Excitation Raman Spectroscopy to Examine Historic Powders Enclosed in Glass Vials. *Sensors* **2022**, *22*, 3560. [CrossRef]
39. Rodriguez, S.H.; Appoloni, C.R.; Campos, P.H.O.V.; Gonçalves, B.; Kajiya, E.A.M.; Molari, R.; Rizzutto, M.A.; Winter, C. Non-Destructive and portable analyses helping the study and conservation of a Saraceni copper plate painting in the São Paulo museum of art. *Microchem. J.* **2020**, *155*, 104787. [CrossRef]
40. Bacci, M. *UV-VIS-NIR, FT-IR and FORS Spectroscopies*; Modern Analytical Methods in Art and Archaeology; Chemical Analysis Series; Ciliberto, E., Spoto, G., Eds.; John Wiley & Sons: New York, NY, USA, 2000; Volume 155, pp. 321–361.
41. Milani, C.; Rosi, F.; Daveri, A.; Brunetti, B.G. Reflation infrared spectroscopy for the non-invasive in situ study of artists' pigments. *Appl. Phisics A Mater. Sci. Process.* **2012**, *100*, 295–307. [CrossRef]
42. Vagnini, M.; Milani, C.; Cartechini, L.; Rocchi, P.; Brunetti, B.G.; Sgamellotti, A. FT-NIR spectroscopy for non-invasive identification of natural polymers and resins in easel paintings. *Anal. Bioanal. Chem.* **2009**, *395*, 2107–2118. [CrossRef]
43. IRUG Database. Available online: https://www.irug.org/ (accessed on 4 January 2024).
44. Corregidor, V.; Oliveira, A.R.; Rodrigues, P.A.; Alves, L.C. Paintings on copper by the Flemish artist Frans Francken II: PIXE characterization by external microbeam. *Nucl. Instrum. Methods Phys. Res. Sect. B Beam Interact. Mater. Atoms* **2015**, *348*, 291–295. [CrossRef]
45. Martin, E.; Eveno, M.; Le Chanu, P. Painting on Copper: Herman van Swanevelt, landscapes with two shepherds and a woman on a donkey. *Kermes Art Conserv. Restor.* **1999**, *12*, 64–66.
46. Van der Weerd, J.; van Loon, A.; Boon, J.J. FTIR studies of the effects of pigments on the aging of oil. *Stud. Conserv.* **2005**, *50*, 3–22. [CrossRef]
47. Carlesi, S.; Picollo, M.; Ricci, M.; Becucci, M. The ageing of model pigment/linseed oil systems studied by means of vibrational spectroscopies and chemometrics. *Vib. Spectrosc.* **2018**, *99*, 86–92. [CrossRef]
48. Bouchard, M.; Smith, D.C. Catalogue of 45 reference Raman spectra of minerals concerning research in art history or archaeology, especially on corroded metals and coloured glass. *Spectrochim. Acta Part A Mol. Biomol. Spectrosc.* **2003**, *59*, 2247–2266. [CrossRef] [PubMed]
49. Morsch, S.; Bastidas, P.D.; Rowland, S.M. AFM-IR insights into the chemistry of interfacial tracking. *J. Mater. Chem. A* **2017**, *5*, 24508–24517. [CrossRef]

50. Genestar, C.; Pons, C. Earth pigments in painting: Characterisation and differentiation by means of FTIR spectroscopy and SEM-EDS microanalysis. *Anal. Bioanal. Chem.* **2005**, *382*, 269–274. [CrossRef]
51. Helwig, K. The Characterisation of Iron Earth Pigments Using Infrared Spectroscopy. In Proceedings of the Second Infrared and Raman Users Group Conference (IRUG2), London, UK, 12–13 September 1995; Victoria & Albert Museum: London, UK, 1995; pp. 83–92.
52. Bikiaris, D.; Daniilia, S.; Sotiropoulou, S.; Katsimbiri, O.; Pavlidou, E.; Moutsatsou, A.P.; Chryssoulakis, Y. Ochre-differentiation through micro-Raman and micro-FTIR spectroscopies: Application on wall paintings at Meteora and Mount Athos, Greece. *Spectrochim. Acta Part A Mol. Biomol. Spectrosc.* **2000**, *56*, 3–18. [CrossRef]
53. Bevilacqua, N.; Borgioli, L.; Gracia, I.A. *I pigmenti Nell'arte: Dalla Preistoria Alla Rivoluzione Industriale*; Il Prato: Padova, Italy, 2010.
54. Vetter, W.; Latini, I.; Schreiner, M. Azurite in medieval illuminated manuscripts: A reflection-FTIR study concerning the characterization of binding media. *Herit. Sci.* **2019**, *7*, 21. [CrossRef]
55. Lluveras, A.; Boularand, S.; Andreotti, A.; Vendrell-Saz, M. Degradation of azurite in mural paintings: Distribution of copper carbonate, chlorides and oxalates by SRFTIR. *Appl. Phys. A Mater. Sci. Process.* **2010**, *99*, 363–375. [CrossRef]